ACS Catalysis

pubs.acs.org/acscatalysis

Research Article

Challenging Metathesis Catalysts with Nucleophiles and Brønsted Base: Examining the Stability of State-of-the-Art Ruthenium Carbene Catalysts to Attack by Amines

Daniel L. Nascimento, Immanuel Reim, Marco Foscato, Vidar R. Jensen, and Deryn E. Fogg*

Cite This: *ACS Catal.* 2020, 10, 11623−11633

Read Online

ACCESS | Metrics & More | Article Recommendations | Supporting Information

ABSTRACT: Critical to advancing the uptake of olefin metathesis in leading contexts, including pharmaceutical manufacturing, is identification of highly active catalysts that resist decomposition. Amines constitute an aggressive challenge to ruthenium metathesis catalysts. Examined here is the impact of 1,8-diazabicyclo[5.4.0]undec-7-ene (DBU), morpholine, *n*-butylamine, and triethylamine on Ru metathesis catalysts that represent the current state of the art, including cyclic alkyl amino carbene (CAAC) and N-heterocyclic carbene (NHC) complexes. Accordingly, the amine-tolerance of the nitro-Grela catalyst $RuCl_2(H_2IMes)(=CHAr)$ (**nG**; Ar = C_6H_4-2-O^{i}Pr-5-NO_2) is compared with that of its CAAC analogues **nGC1** and **nGC2**, and the Hoveyda-class catalyst $RuCl_2$(**C2**)(=CHAr′) **HC2** (Ar′ = C_6H_4-2-O^{i}Pr). In **C1**, the carbene carbon is flanked by an *N*-2,6-$Et_2C_6H_3$ group and a CMePh quaternary carbon; in **C2**, by an *N*-2-^{i}Pr-6-MeC_6H_3 group and a CMe_2 quaternary carbon. The impact of 1 equiv amine per Ru on turnover numbers (TONs) in ring-closing metathesis of diethyl diallylmalonate was assessed at 9 ppm Ru, at RT and 70 °C. The deleterious impact of amines followed the trend $NEt_3 \sim NH_2{}^n$Bu ≪ DBU ~ morpholine. Morpholine is shown to decompose **nGC1** by nucleophilic abstraction of the methylidene ligand; DBU, by proton abstraction from the metallacyclobutane. Decomposition was minimized at 70 °C, at which **nGC1** enabled TONs of ca. 60 000 even in the presence of morpholine or DBU, vs ca. 80 000 in the absence of base. Unexpectedly, H_2IMes catalyst **nG** delivered 70−90% of the performance of **nGC1** at high temperatures, and underwent decomposition by Brønsted base at a similar rate. Density functional theory (DFT) analysis shows that this similarity is due to comparable net electron donation by the H_2IMes and **C1** ligands. Catalysts bearing the smaller **C2** ligand were comparatively insensitive to amines, owing to rapid, preferential bimolecular decomposition.

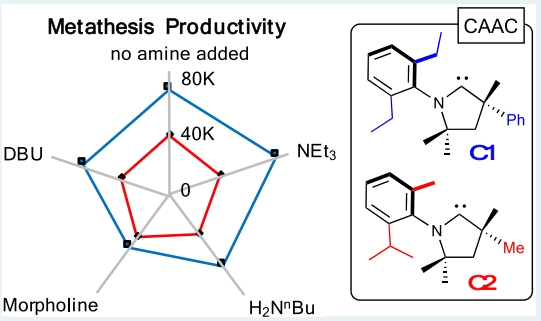

KEYWORDS: *olefin metathesis, catalyst decomposition, deprotonation, metallacyclobutane, amine, nucleophile, carbene, DFT*

INTRODUCTION

Olefin metathesis offers exceptionally versatile catalytic tools for the assembly of carbon−carbon bonds.[1] Widely embraced in organic synthesis, metathesis methodologies have now begun to emerge in pharmaceutical manufacturing, particularly for the production of antiviral therapeutics.[2] Among the most important catalysts used in the latter context is the nitro-Grela complex **nG** (Chart 1),[3] which is stabilized by an N-heterocyclic carbene (NHC) ligand.

Large-scale implementation, however, brings new demands for robustness, reliability, and mechanistic understanding (the latter encompassing both intended and unintended chemistries).[4a] From this perspective, olefin metathesis falls short of other catalytic methodologies, such as hydrogenation and cross-coupling, which are now mainstays of pharmaceutical manufacturing.[4] Grubbs' pioneering development of ruthenium metathesis catalysts,[5] with their dramatically improved tolerance for oxygen and water relative to their group 6 predecessors, was *the* development that put olefin metathesis into the hands of the practicing organic chemist. Nevertheless, reports of the instability of the active species date back nearly 20 years.[6] Like the majority of metathesis catalysts, the Ru-NHC catalysts readily degrade via *β*-elimination of the metallacyclobutane (MCB) ring from **Ru-1** (Scheme 1a),[7] and bimolecular coupling of [Ru]=CHR intermediates (Scheme 1b).[7,8]

These challenges provide context for the breakthrough importance of cyclic alkyl amino carbene (CAAC) derivatives that resist *β*-elimination,[9] notwithstanding efforts to reverse catalyst decomposition.[10] Dramatically higher turnover numbers (TONs) have been achieved with Ru-CAAC catalysts, relative to their NHC predecessors, in high-profile applications

Received: June 24, 2020
Revised: August 29, 2020
Published: September 8, 2020

https://dx.doi.org/10.1021/acscatal.0c02760
ACS Catal. 2020, 10, 11623−11633

Chart 1. Metathesis Catalysts Discussed

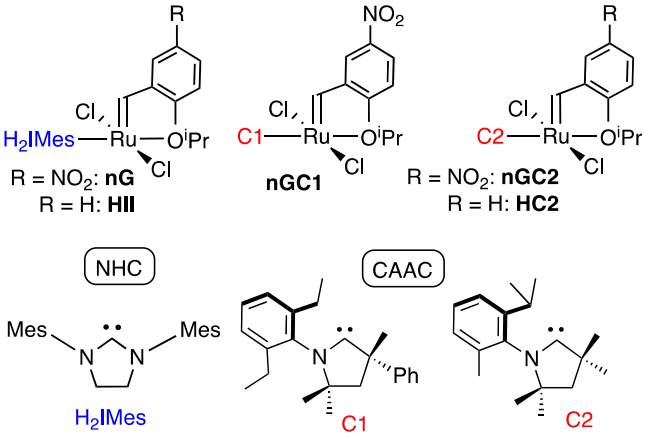

that include macrocyclization and the production of α-olefins from renewable oleate esters.[11] Importantly, the improved productivity achieved by shutting down β-elimination permits use of lower catalyst concentrations, which in turn diminishes bimolecular decomposition. The resulting step-change in efficiency has the further potential to alleviate challenges to continuous−flow metathesis.[12]

To date, however, little study has focused on the susceptibility of the CAAC catalysts to decomposition by exogenous agents.[13,14] Of particular importance are amines. Amines may be present as minor contaminants (for example, morpholine is reportedly present in parts per million (ppm) levels in technical-grade toluene),[14a] or as functional groups on the substrate. In the latter case, they are present in very high proportions relative to the catalyst. The ubiquity of nitrogen centers in active pharmaceutical ingredients (APIs) underscores the importance of understanding their unintended reaction chemistry.[15] Even trace amines can have a major impact on the viability of metathesis reactions. Morpholine and 1,8-diazabicyclo[5.4.0]undec-7-ene (DBU) contaminants were shown to severely degrade the performance of early ruthenium catalysts in process chemistry campaigns at Boehringer-Ingelheim[14a] and GlaxoSmithKline.[14b] More generally, problematic catalyst performance has led to the widespread adoption of protection strategies for primary or secondary amines and amides,[16] as well as pyridines.[17]

Scheme 1. Major Intrinsic Decomposition Pathways Established for Ru-H_2IMes Metathesis Catalysts[a]

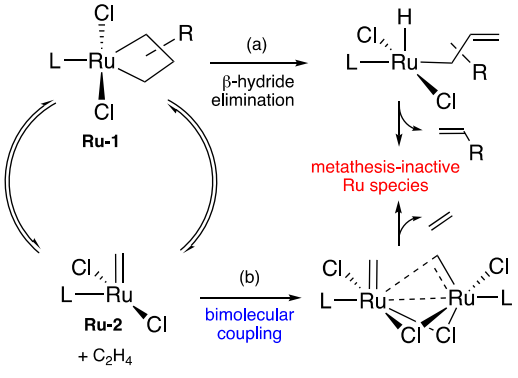

[a]An additional ring-expansion pathway has been established for olefins bearing an α-alkyl substituent.[10a]

We have established two major pathways by which amines attack the metathesis-active species. These are deprotonation of **Ru-1** (by, e.g., DBU; Scheme 2a),[18] and nucleophilic abstraction of the methylidene ligand from **Ru-2** (by, e.g., $NH_2{}^nBu$; Scheme 2b; related chemistry has been established for PCy_3-stabilized catalysts).[18−20]

Scheme 2. Amine-Induced Decomposition Pathways

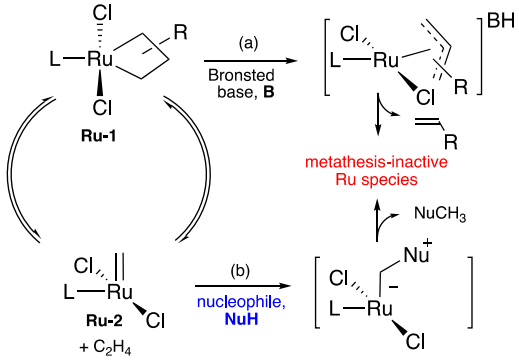

These pathways are curtailed where amine basicity and nucleophilicity are limited. For example, anilines are not only compatible with Ru-catalyzed metathesis, but can be valuable ancillary ligands.[21] Tertiary amines are likewise widely regarded as innocuous, owing to steric protection of the nitrogen site,[16a,b] but scattered reports (including recent model studies)[18,22] suggest that even these may trigger catalyst decomposition. Here we examine the productivity of leading NHC and CAAC catalysts (Chart 1) when challenged by amines of varying size, basicity, and nucleophilicity.

RESULTS AND DISCUSSION

Impact of Amines on Metathesis Productivity. In the present work, we focused on the impact of amines of widely differing bulk and basicity.[23] Three of these have been established as problematic in pharma and elsewhere (see Chart 2 and discussion above). As well, NEt_3 was evaluated, in

Chart 2. Amines Examined, and pK_a of the Conjugate Acid

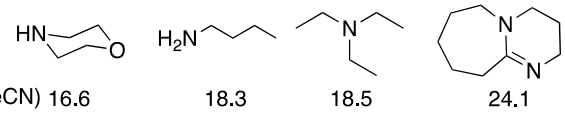

pK_a (MeCN)	16.6	18.3	18.5	24.1

light of ambiguities concerning whether tertiary amines are in fact innocuous.[18,22] Catalysts surveyed are selected as representing the current state of the art: they include the CAAC complexes **nGC1**, **nGC2**, and **HC2** (which afford the highest metathesis TONs reported[11] to date), and the important, widely used NHC analogue **nG**.

The benchmark substrate diethyl diallylmalonate (**1**, Figure 1) was chosen for these studies because its exceptional ease of cyclization means that any agents that inhibit ring-closing metathesis (RCM) merit attention. Reactions were conducted in toluene (now the most widely used solvent for metathesis),[22b] in the presence of 1 equiv amine per Ru. In the TON studies, we employed catalyst loadings of 9 ppm (0.0009 mol % Ru), both to ensure that the impact of added amine is not masked by excessive catalyst loadings, and to approximate targeted catalyst loadings. To assess whether heat

https://dx.doi.org/10.1021/acscatal.0c02760
ACS Catal. 2020, 10, 11623−11633

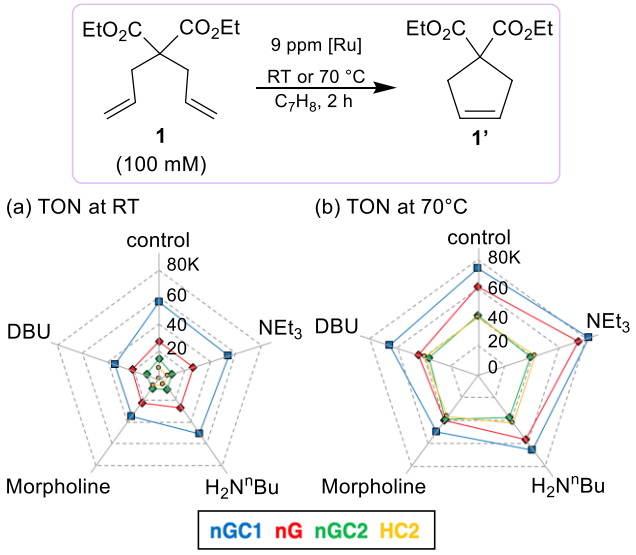

Figure 1. Radar plots showing the impact of amines on TONs (1 equiv vs Ru). (a) At RT: TON_{max} ca. 60 000. (b) At 70 °C: TON_{max} ca. 80 000. For expanded plots and numerical data, see the Supporting Information (SI).

reinforces or mitigates negative impacts, RCM was carried out at 25 and 70 °C.

The radar plots of Figure 1 give a direct visual comparison of productivity for all four catalysts, and the impact of amine on each. The maximum TON attained in the *absence* of amine is indicated on the vertical radial line, with each of the remaining "spokes" depicting the impact of a specific amine. Greater deviations from the outermost point toward the center signify lower productivity, i.e., a greater negative impact.

As no direct comparison of all four catalysts has previously been reported, we begin by analyzing their performance in the control reaction: that is, in the absence of amine (vertical spoke). The outermost data-point on the pentagonal line indicates the maximum TON achieved using the top-performing catalyst **nGC1**: 56 700 at RT (Figure 1a), or 74 400 at 70 °C (Figure 1b). The maximum TON for H_2IMes analogue **nG**, in comparison, was 27 800 or 61 100, at RT or 70 °C, respectively. The drop relative to **nGC1** reflects the vulnerability of the NHC catalysts to β-hydride elimination (see Scheme 1a), a decomposition pathway to which the CAAC catalysts are nearly immune.[9] Of note, however, the difference in performance between **nG** and **nGC1** is far less in this reaction than in the more challenging contexts noted above.

Least productive were **nGC2** and **HC2**, with TONs of 14 400 and 7800, respectively (a difference that disappears at higher temperatures, as the slower initiation of **HC2** is erased: both catalysts then deliver a TON of ca. 40 000). We attribute this drop in productivity to the poor steric protection conferred by the small quaternary CMe_2 group of **C2**, and consequently faster bimolecular decomposition (Scheme 1b). Such coupling has been shown to be dramatically faster for the **C1** methylidene complex than its H_2IMes analogue **Ru-2**.[11e,24] While bimolecular decomposition of the **C2** derivative has not been directly examined, the fact that TONs *decrease* for **C2** derivatives when catalyst loadings are tripled from 1 to 3 ppm suggests an even greater vulnerability with a decreasing CAAC size.[11b]

The trend in catalyst productivity was unaffected in the presence of amine, with **nGC1** remaining most productive. A deleterious impact was observed in all cases, however, increasing in the order $NEt_3 \sim NH_2{}^nBu \ll$ morpholine ~ DBU. For $NH_2{}^nBu$ and NEt_3, this impact was relatively minor. This is important given model studies with Ru-H_2IMes catalysts, which indicated nucleophilic abstraction of the methylidene ligand by $NH_2{}^nBu$,[19] and MCB deprotonation by NEt_3,[18] on reaction with 10 equiv styrene and amine. The present work demonstrates that under conditions more relevant to catalysis, decomposition by 1 equiv NEt_3 and $NH_2{}^nBu$ does not significantly compete with metathesis. Morpholine and DBU caused greater declines in TON (ca. 40% at RT for **nGC1**), but this could generally be mitigated by use of high temperatures, most significantly for DBU.

Also noteworthy is the beneficial impact of small proportions of NEt_3 at 70 °C: this increased TONs relative to the base-free control by ca. 10%, for both **nGC1** and **nG**.[25] Improved TONs were likewise observed for an independent batch of **1**, albeit at a slightly lower level. In contrast, no improvement was seen for two other substrates (styrene and a pro-lactone; see Table S1b), suggesting that the beneficial impact of NEt_3 is due to suppression of contaminants present in **1**. Beller, Kadyrov, and co-workers have noted that diene **1**, despite its benchmark status, contains a wide range of contaminants (including butanedioic acid and 2-acetyl-2-allylpent-4-enoic acid).[26] They established the beneficial impact of several additives, although amines were omitted. The observed decline in TONs when a larger excess of NEt_3 was added[25] presumably reflects MCB deprotonation. We previously demonstrated that NEt_3 is able to deprotonate **Ru-1**, albeit more slowly than stronger bases such as Proton Sponge.[18a]

The discussion so far has focused on the core issue from a synthetic perspective: identification of catalysts and conditions that deliver highest TON despite the presence of amine. **nGC1** emerges as the top-performing candidate, and high temperatures as beneficial. Unexpectedly, however, the H_2IMes catalyst **nG** does not fall far short, delivering 70−90% of the TONs of **nGC1** at 70 °C. This contrasts with the orders-of-magnitude superiority of CAAC vs NHC catalysts in ethenolysis, and their ca. 5-fold superiority in mRCM.[27]

Also striking is the performance of the **C2** catalysts, for which Figure 1b indicates essentially no impact by any amine at 70 °C. This "tolerance" is due to much faster decomposition by amine-independent pathways, most probably bimolecular decomposition, to which these sterically less protected catalysts are particularly susceptible, as noted above. Catalyst decomposition has previously been shown to follow unique pathways for sufficiently small carbene ligands.[28] Given that other decomposition pathways overtake those induced by amine in the present case, the **C2** catalysts are omitted from further analysis.

If stronger σ-donation results in a more electron-rich Ru center for the CAAC catalysts vs their H_2IMes analogues, **nGC1** might be expected to resist attack by nucleophiles or Brønsted base to a greater extent than **nG**. To probe this point, we plot in Figure 2 the amine-tolerance of **nGC1** and **nG** independent of inherent catalyst productivity: that is, as the percent of activity retained in the presence of amine. Unexpectedly, comparable amine-tolerance is evident, despite the steric and electronic distinctions between the **C1** and the H_2IMes ligands. Although **nGC1** is slightly more sensitive to

https://dx.doi.org/10.1021/acscatal.0c02760
ACS Catal. 2020, 10, 11623−11633

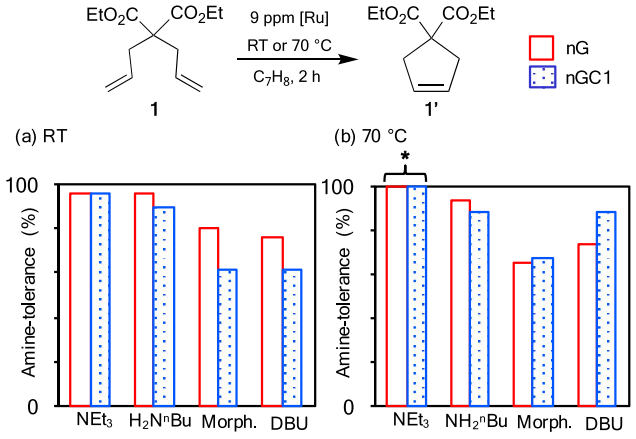

Figure 2. Amine-tolerance of **nG** and **nGC1** in RCM of **1** (100 mM). (a) At RT. (b) At 70 °C. Amine-tolerance = $[100 - (TON_{control} - TON_{amine})/TON_{control}] \times 100$. *The value for NEt_3 in (b) exceeds 100 (**nG**: 122%; **nGC1**: 110%), indicating that the TON is higher than that in the control experiment; see discussion in the text.

morpholine and DBU at RT, the differences are erased at 70 °C; indeed, the CAAC catalyst exhibits slightly higher stability to DBU. This point is examined computationally below.

A final set of experiments examined important mechanistic points for the two most deleterious amines. Here we wished to extract the rate at which DBU decomposes **nG** and **nGC1**, relative to the background β-hydride elimination, and to establish the pathway by which morpholine effects decomposition. The decomposition pathway for DBU was previously examined for **HII**. Unsurprisingly, given the high basicity of DBU (by far the strongest base examined; see the pK_a values of Chart 1), it deprotonates the metallacyclobutane intermediate **Ru-1** (Scheme 2a).[18] An important question, however, is the rate of deprotonation relative to competing β-H elimination (Scheme 1a). Both reactions liberate propenes. To assess their respective rates, we measured the total yield of propenes during metathesis of styrene, and subtracted that formed via β-hydride elimination (Figure 3).

Deprotonation is clearly much faster than β-H elimination for **nG**, as indicated by the elimination of >50% propenes within 5 min in the presence of DBU, vs 2% in its absence. Disappearance of alkylidene signals is complete in 30 min. In comparison, 34% deprotonation is seen within 5 min for the CAAC catalyst **nGC1** (which, as noted above, undergoes essentially no β-H elimination). Deprotonation reaches nearly 60% by 30 min. This should be viewed as a lower limit, however, given the propensity to competing bimolecular coupling at the 20 mM Ru concentrations required for this experiment.[9] The latter accounts for the plateau in propene yields at ca. 10 min. Nevertheless, it appears that **nG** and **nGC1** are readily attacked by DBU (Figure 3c), at broadly similar rates. This implies that the distinct electronic properties of the CAAC ligand[29−31] do not greatly affect the vulnerability of the MCB. This point is probed by computational analysis in the final section.

The mechanism by which morpholine decomposes metathesis catalysts, somewhat surprisingly, has not been explored. Only ca. 5% propenes were observed on repeating the experiment of Figure 3 with **nGC1** and morpholine (Figure S2). MCB deprotonation is evidently a minor pathway, consistent with the low basicity of morpholine indicated in Chart 2. We therefore examined the possibility that morpho-

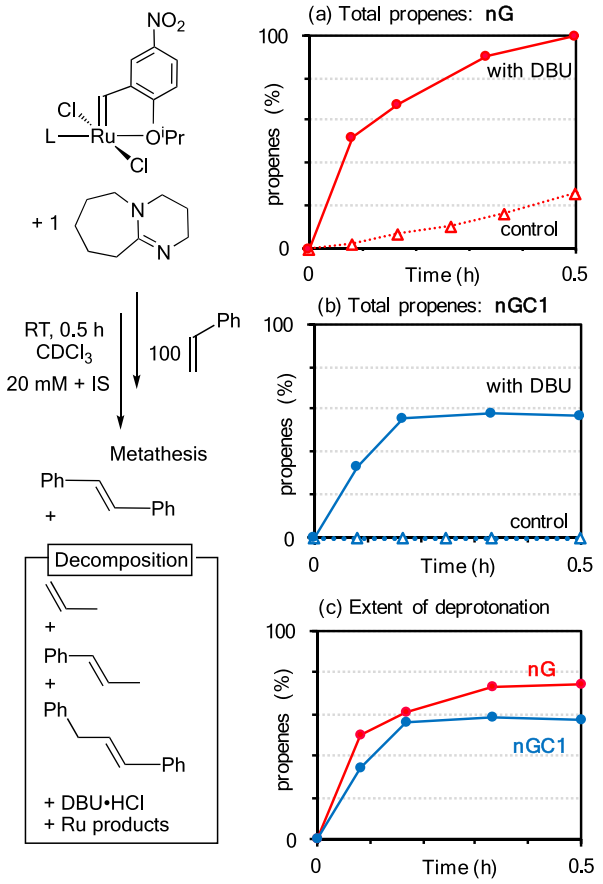

Figure 3. Assessing rates of MCB deprotonation relative to β-H elimination for **nG** and **nGC1** (NMR analysis; 20 mM Ru), showing propene products and yields. Control reaction = β-H elimination.

line engages in nucleophilic abstraction of the methylidene group from **Ru-2**, as previously shown for the primary amine $NH_2{}^nBu$ (Scheme 2b).[18b]

To probe this point, a CAAC derivative of the Piers catalyst (see **Piers-C1**, Scheme 3) was treated with ethylene at −45 °C

Scheme 3. Confirming Methylidene Abstraction by Morpholine

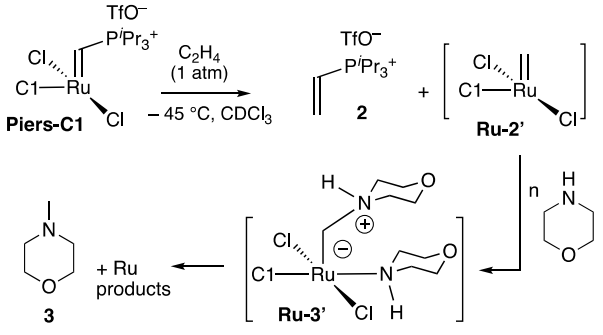

in $CDCl_3$. Because the Piers catalysts initiate irreversibly (that is, the bulky phosphonium ylide released from the benzylidene resists reuptake), they afford clean entry to the active species. Injection of cold morpholine caused the solution to immediately change color from dark red to orange-brown, and an alkylidene signal assigned to a morpholine adduct was detected at 18.57 ppm.[7a,9] After warming to 25 °C to complete formation and decomposition of the **Ru-3′** intermediate, *N*-

https://dx.doi.org/10.1021/acscatal.0c02760
ACS Catal. 2020, 10, 11623−11633

methylmorpholine **3** was observed in 43% yield. The balance is presumed to be due to bimolecular coupling, which is markedly more aggressive for the **C1** derivative **Ru-2′** than its H_2IMes analogue.[9] Neither propenes nor morpholine·HCl from deprotonation of **Ru-1′** were observed, consistent with the deleterious role of morpholine stemming from its nucleophilicity, rather than its Brønsted basicity.

Computational Studies. Density functional theory (DFT) analysis was undertaken to probe the susceptibility of **Ru-1** to deprotonation by DBU, as compared to β-elimination or continued metathesis (i.e., retro-addition to eliminate ethylene). These pathways, with the corresponding energy barriers in brackets, are shown in Scheme 4. Deprotonation of

Scheme 4. Calculated Free Energies for Reactions of the MCB Intermediate Ru-1: (a) Metathesis (Retro-addition); (b) β-Hydride Elimination; (c) Deprotonation by DBU[a]

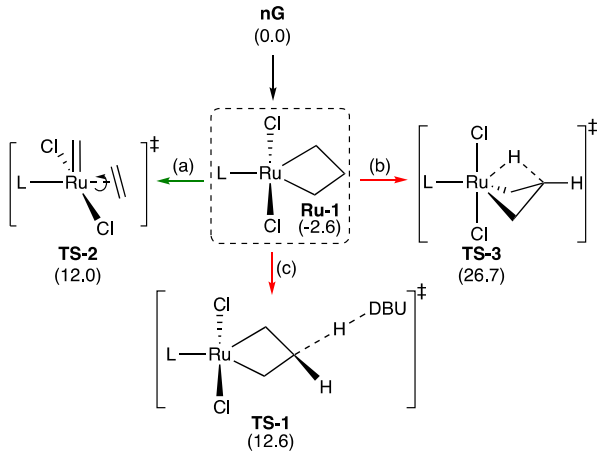

[a]Given in brackets are activation free energies (kcal/mol) vs **nG**, calculated using the PBE-D3BJ-SMD computational model with chloroform as the solvent. For details and additional results, see SI and Table S3.

Ru-1 led to a single transition state for proton transfer to DBU (**TS-1**), with a free energy of 12.6 kcal/mol relative to **nG**, as compared to 12.0 kcal/mol for concerted bond breaking and rotation of ethylene (which represents the upper bound for continued metathesis; see SI), and 26.7 kcal/mol for β-elimination. Thus, deprotonation is predicted to be much faster than β-elimination, in agreement with the experimental results in Figure 3.

For the CAAC system, the complexity of analysis is significantly increased by the lack of symmetry in the **C1** ligand. We therefore focused on assessing the barrier to deprotonation of the metallacyclobutane **Ru-1′**, for comparison with the H_2IMes system. Proton transfer to DBU from **Ru-1′** can proceed via four isomers of comparable energy (**TS-1a′−d′**; Table S3). The calculated free energy barriers for deprotonation were 14−20 kcal/mol relative to the precatalyst, depending on the isomer, solvent, and functional. Importantly, however, the barrier for the most favorable pathway from **nGC1** is very similar to that for **nG** (within 1.4 kcal/mol, relative to the precatalyst, or 0.3 kcal/mol, relative to the MCB). DBU is thus predicted to deprotonate the MCB at similar rates for each carbene complex, as indeed observed experimentally.

The thermodynamics of proton abstraction likewise indicate similar acidity for the **C1** and H_2IMes intermediates. To exploit error cancellation, we evaluated the energetics of the acid−base equilibrium between each MCB and its conjugate base, the allylic anion **Ru-4** or **Ru-4′** (Scheme 5). With a

Scheme 5. Assessing Relative Acidity of the MCB β-H for the C1 and H_2IMes Systems[a]

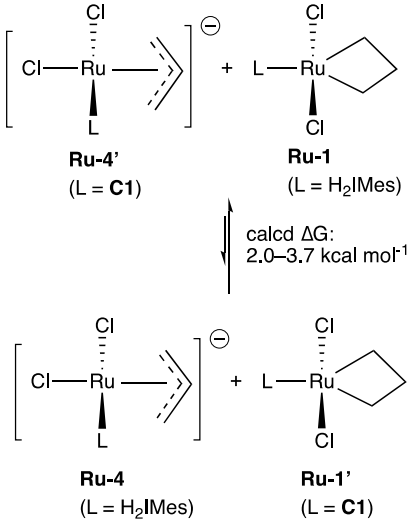

[a]Calculated using the PBE-D3BJ-SMD computational model with chloroform as the solvent; see Tables S4 and S5 for additional data.

calculated reaction Gibbs free energy of 2.0−3.7 kcal/mol, depending on the computational model used (Table S5), the equilibrium favors the deprotonated **C1**-complex **Ru-4′** to a small extent. In short, the acidity of the **nG** and **nGC1** MCB intermediates is predicted to be comparable.

The similar propensity of the **nG** and **nGC1** systems to deprotonation by base was initially unexpected. Although CAAC ligands are better π-acceptors than NHCs, their net electron-donor capacity (that is, the difference between σ-donation and π-back-donation) is consistently described as better than that of NHC ligands.[29] Increased electron donation from the carbene might be expected to reduce the acidity of the MCB β-proton in **nGC1**. However, minimal differences are seen in the Tolman electronic parameter (TEP; the ν(CO) stretching frequencies of $Ni(CO)_3(L)$ complexes)[32] for representative CAACs and their NHC counterparts,[30,33] suggesting that any increase in overall donating capacity for the CAACs may be modest.

Natural charge analysis indeed indicates that **C1** and H_2IMes donate essentially the same number of electrons in the MCB intermediate (0.496 for **Ru-1**, and 0.484 for **Ru-1′**; Tables S6 and S7). Thus, despite the significant differences in the electronic properties of the CAAC and NHC ligands, the better σ-donor capacity of the CAACs is offset by their better π-acceptor properties.[29,30] Comparable net electron donation to the ruthenacyclobutane fragment of **nG** and **nGC1** accounts for their similar susceptibility to proton abstraction by base.

CONCLUSIONS

Amines are ubiquitous as functional groups and contaminants in olefin metathesis. The foregoing describes the impact of selected amines on state-of-the-art catalysts containing CAAC and NHC ligands. The amines studied were chosen for the documented risk they pose to metathesis productivity, or, in the case of the tertiary amine NEt_3, to test a widely presumed

https://dx.doi.org/10.1021/acscatal.0c02760
ACS Catal. 2020, 10, 11623−11633

innocuousness. The order of increasing negative impact was NEt_3 ~ $NH_2{}^nBu$ ≪ morpholine ~ DBU, with NEt_3 and $NH_2{}^nBu$ showing very minor effects, and DBU and morpholine being much more damaging. In general, deleterious effects diminished at elevated temperatures. The impact of amine does not group by mode of decomposition. Thus, NEt_3 and DBU, both of which act by deprotonating the MCB, represent the least and one of the most deleterious amines, respectively, and regardless of temperature. Similarly, morpholine is much more aggressive than the primary amine $NH_2{}^nBu$, although both decompose the catalysts by nucleophilic attack on the [Ru]=CHR moiety.

The CAAC catalyst **nGC1** proved most productive in the presence of amine, with TONs of ca. 50 000 to 80 000. Unexpectedly, competitive performance was observed for the H_2IMes analogue **nG**, which delivered TONs ranging from 70−90% of those attained with **nGC1**. The difference in TONs between the CAAC and NHC catalysts in the test reaction employed here (RCM of diethyl diallylmalonate **1**) is much less substantial than in more challenging reactions, however, and a greater margin of difference in amine-sensitivity may thus be apparent in other contexts. Nevertheless, **nG** and **nGC1** were found to undergo deprotonation by base at broadly comparable rates. On the basis of DFT calculations, this similarity is attributed to comparable net electron donation by the H_2IMes and **C1** ligands. The Ru centers in the metallacyclobutane intermediates are consequently comparably electron-rich, and the β-protons of the MCB are hence similar in their acidity and susceptibility to abstraction by base.

Finally, the **C2** catalysts were found to be least productive, but also least sensitive to amines. A simple explanation accounts for this initially puzzling observation: it does not indicate that the smaller **C2** catalysts are in fact immune to attack by amine, but that bimolecular decomposition is considerably faster. The latter reaction thus outcompetes amine-induced decomposition where the carbene is sufficiently small.

EXPERIMENTAL AND COMPUTATIONAL SECTION

General Experimental Procedures. Reactions were carried out under N_2 using glovebox or Schlenk techniques, unless otherwise noted. Toluene (Fisher, high-performance liquid chromatography (HPLC) grade) was distilled over P_2O_5 and stored under N_2 over 4 Å molecular sieves for at least 18 h prior to use. $CDCl_3$ (Cambridge Isotopes) was degassed by 5 freeze/pump/thaw cycles and stored as above. Diethyl diallylmalonate (**1**, TCI, 98%), dodecane (Sigma >99%) and styrene (**3**, Sigma, >99%) were degassed similarly and stored in the glovebox freezer (−35 °C). $NH_2{}^nBu$ (Alfa, 99%), morpholine (Sigma, >99.5%), DBU (Alfa, 99%), and NEt_3 (Sigma, >99.5%) were degassed and stored under N_2. Literature methods were used to prepare diene **2**,[34] macrolactone **2′**,[34] and catalysts **nGC2**,[11d] **HC2**,[11a] **nG**,[3] and **Piers-C1**;[9] **nGC1** was kindly supplied by Apeiron Synthesis. Ethylene (BOC Gases; Linde, 99.9%) and the internal standard dimethyl terephthalate (DMT, Aldrich, 99%) were used as received.

^{1}H NMR spectra were recorded on an Advance II 500 spectrometer at 23 °C, unless otherwise specified. Chemical shifts are reported in ppm and referenced to the residual proton signal of the deuterated solvent. RCM experiments were analyzed using an Agilent 7890A gas chromatograph (GC) equipped with an autosampler, flame ionization detector (FID), and Agilent HP-5 polysiloxane column (30 m length, 320 μm diameter). Calibration curves of peak areas versus concentrations were established for substrates and products in the relevant concentration regimes, using ca. 1:1 (w/w) sample versus dodecane as the internal standard; for NMR analysis they were confirmed by integration vs dodecane.

Catalysis Experiments. Stock solutions of each amine were prepared by dissolving 2.0 μL of the amine in C_7H_8 (20.0 mL) and diluting a 1.0 mL aliquot to 10.0 mL with C_7H_8. All were stored in a glovebox freezer (−35 °C) and allowed to come to thermal equilibrium at RT for ca. 20 min before use. For experiments probing the impact of amines, these stock solutions were added immediately prior to catalyst addition. Stock solutions of the catalyst were prepared immediately prior to use (10 mg of the catalyst in 20.0 mL of C_7H_8 and diluting a 1.0 mL aliquot to 10.0 mL with C_7H_8). Heated reactions were carried out in a degassed oil bath in the glovebox at 70 ± 1 °C, with thermal equilibration for 10 min prior to catalyst addition.

Representative Procedure for RCM of Diethyl Diallylmalonate (1) with nGC1. (a) Control experiment: To **1** (97.0 μL, 0.400 mmol) and dodecane (91.0 μL, 0.400 mmol, 1 equiv; internal standard for GC analysis) was added 3.76 mL of C_7H_8 to give a final concentration of 100 mM **1**. A 100 μL aliquot was removed for GC-FID analysis to establish the initial ratio of **1** to dodecane. To the stirred solution was added **nGC1** (49.0 μL of a stock solution of 10 mg of **nGC1** in 200 mL; serial dilution, see above; 3.6 nmol, 0.0009 mol %). After 2 h, an aliquot was removed, quenched with KTp[35] (10 mg/mL in tetrahydrofuran (THF); 10 equiv vs starting Ru), and analyzed by GC-FID. (b) $NH_2{}^nBu$: As above, with $NH_2{}^nBu$ (36.0 μL, 3.64 nmol, 1 equiv) and 3.73 mL of C_7H_8. (c) Morpholine: As above, with morpholine (32.0 μL, 3.66 nmol, 1 equiv) and 3.73 mL of C_7H_8. (d) DBU: As above, with DBU (54.0 μL, 3.61 nmol, 1 equiv) and 3.71 mL of C_7H_8. (e) NEt_3: As above, with 1 or 10 equiv of NEt_3 (50.0 μL, 3.60 nmol, 1 equiv in 3.71 mL of C_7H_8, or 502 μL, 36.0 nmol, 10 equiv in 3.26 mL of C_7H_8). For the radar plots, see Figure 1; for numerical data, see Tables S1a and S2.

Representative Procedure for RCM of Pro-lactone 2 with nGC1. (a) Control experiment: As above, using pro-lactone **2** (22.8 μL, 0.075 mmol) and dodecane (17.0 μL, 0.075 mmol, 1 equiv) diluted with 14.9 mL of C_7H_8 to a final concentration of 5 mM **2**. To the stirred solution was added a solution of **nGC1** (30.8 μL of a stock solution of 10 mg of **nGC1** in 200 mL; serial dilution, see above; 2.25 μmol, 0.003 mol %). (b) NEt_3: As in the control experiment, with NEt_3 (31.4 μL, 2.25 μmol, 1 equiv). For numerical data, see Table S1b.

Representative Procedure for Self-Metathesis of Styrene 3 with nGC1. (a) Control experiment: As above, using styrene **3** (91.7 μL, 0.800 mmol) and dodecane (182 μL, 0.800 mmol, 1 equiv) diluted with 3.11 mL of C_7H_8 to give a final concentration of 200 mM **3**. Catalyst: **nGC1** (54.8 μL of a stock solution of 10 mg of **nGC1** in 20 mL; 0.040 μmol, 0.005 mol %). (b) NEt_3: As in the control experiment, with NEt_3: 558 μL, 0.040 μmol, 1 equiv. For numerical data, see Table S1b.

Representative Procedure: MCB Decomposition by β-Elimination. (a) From **nGC1**: In a minor adaptation of the reported method,[9] **nGC1** (30 mg, 0.044 mmol) and ca. 10 mg of DMT (0.051 mmol, 1 equiv) were dissolved in $CDCl_3$ (1.69 mL) in a J-Young NMR tube. The **nGC1**/IS ratio was measured (^{1}H NMR). Styrene (500 μL, 4.36 mmol, 100 equiv)

https://dx.doi.org/10.1021/acscatal.0c02760
ACS Catal. 2020, 10, 11623−11633

was added (glovebox) to give a solution of 20 mM in Ru and the timer was immediately started. The NMR tube was shaken periodically over 30 min and then attached to a mechanical rotator (10 rpm) for sustained mixing. (b) From **nG**: As above, with **nG** (30 mg, 0.045 mmol). (c) From **nGC2**: As above, with **nGC2** (27 mg, 0.043 mmol).

Representative Procedure: MCB Decomposition by Deprotonation. (a) From **nGC1**: As above, with **nGC1** (30 mg, 0.044 mmol), DMT (10 mg, 0.051 mmol, 1 equiv), $CDCl_3$ (1.69 mL), styrene (500 μL, 4.36 mmol, 100 equiv), and DBU (6.6 μL, 0.045 mmol, 1 equiv). (b) From **nG**: As above, with **nG** (30 mg, 0.045 mmol), DMT (10 mg, 0.051 mmol, 1 equiv), $CDCl_3$ (1.69 mL), styrene (500 μL, 4.36 mmol, 97 equiv), and DBU (6.7 μL, 0.045 mmol, 1 equiv).

Assessing Methylidene Abstraction from Piers-C1 by Morpholine. To **Piers-C1** (15 mg, 0.018 mmol) and DMT (ca. 10 mg, 0.020 mmol, 1 equiv) in a J-Young NMR tube was added $CDCl_3$ (0.6 mL). The initial ratio of **Piers-C1**/IS was measured and the NMR sample was transferred to a Kontes flask with a stir bar. The NMR tube was rinsed with 0.4 mL of $CDCl_3$, the washings also being transferred to the Kontes flask. The green-brown solution was transferred to the Schlenk line, where it was degassed (FPT; 3×), thawed under ethylene at −45 °C (MeCN-dry ice) to afford a dark red-brown solution, and stirred for 15 min. A chilled (−45 °C) solution of morpholine (4.5 μL, 0.052 mmol, 3 equiv) in 0.8 mL of $CDCl_3$ was then injected, resulting in a final Ru concentration of 9.7 mM. The orange-brown solution was stirred for 20 min, then transferred by a syringe into a prechilled Rotoflo NMR tube, which was inserted into a spectrometer set to −40 °C for ^{1}H NMR analysis. The probe was warmed to 25 °C and the sample was allowed to thermally equilibrate for 10 min prior to ^{1}H NMR analysis.

Computational Details. Density functional theory (DFT) calculations were performed with revisions B.01[36] and C.01[37] of the Gaussian 16 suite of programs. For the H_2IMes-coordinated catalyst **nG**, our prior input geometries were adopted.[18a] For the **C1** analogue **nGC1**, these geometries were modified using Spartan 16.[38] Conformational searches were performed using the MMFF force field[39] as implemented in Spartan 16 by freezing the coordination geometry of the Ru center while exploring torsional degrees of freedom for the **C1** ligand. The allylic species were obtained by deprotonation at C_β of the MCBs.

Molecular geometries were optimized using the ωB97XD functional,[40] which generates geometries for ruthenium metathesis catalysts and other homogeneous catalysts in very good agreement with those of X-ray diffraction.[41] Numerical integration was performed using the Gaussian "ultrafine" grid using valence double-ζ quality basis sets (see below). For the Ru atoms, the Stuttgart/Cologne 28-electron relativistic effective core potentials (ECP28MDF)[42] with the corresponding correlation-consistent valence double-ζ plus polarization basis set (cc-pVDZ-PP)[42] were used as obtained from the Stuttgart/Cologne basis set repository.[43] All other atoms were described by correlation-consistent valence double-ζ plus polarization basis sets (labeled cc-pVDZ[44] at the EMSL basis set exchange website).[45] All geometries were optimized without symmetry constraints to match default convergence criteria (max force $<4.5 \times 10^{-4}$ au, max RMS force $<3.0 \times 10^{-4}$ au, max displacement $<1.8 \times 10^{-3}$ au, and max RMS displacement $<1.2 \times 10^{-3}$ au). Default convergence criteria were used also for the self-consistent field (SCF) procedure (RMS change in the density matrix $<1.0 \times 10^{-8}$ and max change in the density matrix = 1.0×10^{-6}). Stationary points were characterized by the curvature of the analytically calculated second-derivative (Hessian) matrix. Minima were confirmed to have real frequencies only; for transition states, a single imaginary frequency with a mode corresponding to the intended reaction coordinate was confirmed.

Thermal corrections to yield the Gibbs free energies were calculated within the ideal-gas, rigid-rotor, and harmonic oscillator approximations, barring precautions taken to avoid the divergent effects of very soft modes:[46] all frequencies below 100 cm^{-1} were shifted to 100 cm^{-1} when calculating the vibrational component of the entropy (quasi-harmonic oscillator approximation).[46,47]

Single-point (SP) energy calculations were performed in the optimized geometries using the PBE[48] and M06-L[49] functionals in conjunction with the SMD continuum solvent model[50] to account for solvation effects using default parameters for either benzene or chloroform as the solvent. All PBE calculations included Grimme's empirical D3 dispersion corrections with Becke−Johnson (BJ) damping.[51,52] Basis sets of valence quadruple-ζ level quality were used in the single-point calculations: Ru was described by the 28-electron relativistic effective core potential (ECP28MDF)[42] in conjunction with the corresponding correlation-consistent valence quadruple-ζ plus polarization basis set augmented by diffuse functions (cc-pVQZ-PP)[42] from the Stuttgart/Cologne basis set repository.[45] All other atoms were described by correlation-consistent valence quadruple-ζ plus polarization basis sets (cc-pVQZ[44] from the EMSL repository).[45] The single-point SCF convergence criteria were relaxed compared to those of the geometry optimizations (to RMS change in density matrix $<1.0 \times 10^{-5}$, max change in density matrix $<1.0 \times 10^{-3}$).

Free energies in solution were calculated from the following:

$$G_X = E_X + \Delta G^{T=298.15\ K}_{\omega 97XD,qh} + \Delta G^{T=298.15\ K}_{1\ atm \rightarrow 1\ M}$$

where E_X is the SP energy calculated with the computational model X, where X = PBE-D3BJ-SMD(solvent) or M06L-SMD(solvent), and the solvent is either chloroform or benzene. $\Delta G^{T=298.15\ K}_{\omega B97XD,qh}$ is the thermal correction to the Gibbs free energy calculated at the geometry-optimization level with the quasi-harmonic oscillator approximation as described above, and $\Delta G^{T=298.15\ K}_{1atm \rightarrow 1M}$ is the standard state correction from the ideal gas at 1 atm to a 1 M solution (but exhibiting infinite-dilution, ideal-gas-like behavior), which is equal to 1.89 kcal/mol at RT.

Natural population analysis (NPA) was performed using the 7.0.7 version of the natural bond orbital (NBO)[53] program and the electron density obtained from the PBE-D3BJ-SMD-($CHCl_3$) SP energy calculations. The sum of the natural charges calculated for the fragment $RuCl_2(C_3H_6)$ in the metallacyclobutane intermediate of **nG** and **nGC1** (Tables S4 and S5) is negative due to the electron donation from H_2IMes and **C1**, respectively: this donation is defined as the number of electrons corresponding to the negative charge for $RuCl_2(C_3H_6)$.

■ ASSOCIATED CONTENT

Supporting Information

The Supporting Information is available free of charge at https://pubs.acs.org/doi/10.1021/acscatal.0c02760.

https://dx.doi.org/10.1021/acscatal.0c02760
ACS Catal. 2020, 10, 11623−11633

NMR spectra, additional computational results, sample input files (PDF)

Calculated molecular models (XYZ)

AUTHOR INFORMATION

Corresponding Author

Deryn E. Fogg − *Center for Catalysis Research & Innovation, and Department of Chemistry and Biomolecular Sciences, University of Ottawa, Ottawa, Canada K1N 6N5; Department of Chemistry, University of Bergen, N-5007 Bergen, Norway;* orcid.org/0000-0002-4528-1139; Email: dfogg@uottawa.ca, dfo025@uib.no

Authors

Daniel L. Nascimento − *Center for Catalysis Research & Innovation, and Department of Chemistry and Biomolecular Sciences, University of Ottawa, Ottawa, Canada K1N 6N5;* orcid.org/0000-0002-9363-2175

Immanuel Reim − *Department of Chemistry, University of Bergen, N-5007 Bergen, Norway;* orcid.org/0000-0001-7448-9572

Marco Foscato − *Department of Chemistry, University of Bergen, N-5007 Bergen, Norway;* orcid.org/0000-0001-7762-6931

Vidar R. Jensen − *Department of Chemistry, University of Bergen, N-5007 Bergen, Norway;* orcid.org/0000-0003-2444-3220

Complete contact information is available at: https://pubs.acs.org/10.1021/acscatal.0c02760

Notes

The authors declare no competing financial interest.

ACKNOWLEDGMENTS

This work was funded by the Natural Sciences and Engineering Research Council of Canada (NSERC) and by the Research Council of Norway (RCN; projects 262370 and 288135). RCN is also thanked for CPU (NN2506K) and storage resources (NS2506K).

REFERENCES

(1) (a) Grela, K. *Olefin Metathesis—Theory and Practice*; Wiley: Hoboken, NJ, 2014. (b) Grubbs, R. H.; Wenzel, A. G. *Handbook of Metathesis*, 2nd ed.; Wiley-VCH: Weinheim, 2015.

(2) (a) Higman, C. S.; Lummiss, J. A. M.; Fogg, D. E. Olefin Metathesis at the Dawn of Uptake in Pharmaceutical and Specialty Chemicals Manufacturing. *Angew. Chem., Int. Ed.* **2016**, *55*, 3552−3565. (b) Farina, V.; Horváth, A. Ring-Closing Metathesis in the Large-Scale Synthesis of Pharmaceuticals. In *Handbook of Metathesis*; Grubbs, R. H.; Wenzel, A. G., Eds.; Wiley-VCH: Weinheim, 2015; Vol. 2, pp 633−658. (c) Fandrick, K. R.; Savoie, J.; Jinhua, N. Y.; Song, J. J.; Senanayake, C. H. Challenges and Opportunities for Scaling the Ring-Closing Metathesis Reaction in the Pharmaceutical Industry. In *Olefin Metathesis—Theory and Practice*; Grela, K., Ed.; Wiley: Hoboken, 2014; pp 349−366.

(3) Michrowska, A.; Bujok, R.; Harutyunyan, S.; Sashuk, V.; Dolgonos, G.; Grela, K. Nitro-Substituted Hoveyda-Grubbs Ruthenium Carbenes: Enhancement of Catalyst Activity through Electronic Activation. *J. Am. Chem. Soc.* **2004**, *126*, 9318−9325.

(4) (a) Hayler, J. D.; Leahy, D. K.; Simmons, E. M. A Pharmaceutical Industry Perspective on Sustainable Metal Catalysis. *Organometallics* **2019**, *38*, 36−46. (b) Ager, D. J.; de Vries, A. H. M.; de Vries, J. G. Asymmetric Homogeneous Hydrogenations at Scale. *Chem. Soc. Rev.* **2012**, *41*, 3340−3380. (c) Magano, J.; Dunetz, J. R. Large-Scale Applications of Transition Metal-Catalyzed Couplings for the Synthesis of Pharmaceuticals. *Chem. Rev.* **2011**, *111*, 2177−2250.

(5) Schwab, P.; Grubbs, R. H.; Ziller, J. W. Synthesis and Applications of $RuCl_2(=CHR')(PR_3)_2$: The Influence of the Alkylidene Moiety on Metathesis Activity. *J. Am. Chem. Soc.* **1996**, *118*, 100−110.

(6) (a) Amoroso, D.; Yap, G. P. A.; Fogg, D. E. Deactivation of Ruthenium Metathesis Catalysts via Facile Formation of Face-Bridged Dimers. *Organometallics* **2002**, *21*, 3335−3343. (b) Amoroso, D.; Snelgrove, J. L.; Conrad, J. C.; Drouin, S. D.; Yap, G. P. A.; Fogg, D. E. An Attractive Route to Olefin Metathesis Catalysts: Facile Synthesis of a Ruthenium Alkylidene Complex Containing Labile Phosphane Donors. *Adv. Synth. Catal.* **2002**, *344*, 757−763. (c) Amoroso, D.; Yap, G. P. A.; Fogg, D. E. The Life, Death, and ROMP Activity of Ruthenium Complexes Containing the Basic, Chelating Diphosphine Bis(Dicyclohexyl)-1,4-Phosphinobutane. *Can. J. Chem.* **2001**, *79*, 958−963. (d) Volland, M. A. O.; Hansen, S. M.; Rominger, F.; Hofmann, P. Synthesis, Structure, and Reactivity of Cationic Ruthenium(II) Carbene Complexes with Bulky Chelating Bisphosphines: Design of Highly Active Ring Opening Metathesis Polymerization (ROMP) Catalysts. *Organometallics* **2004**, *23*, 800−816. (e) Burdett, K. A.; Harris, L. D.; Margl, P.; Maughon, B. R.; Mokhtar-Zadeh, T.; Saucier, P. C.; Wasserman, E. P. Renewable Monomer Feedstocks via Olefin Metathesis: Fundamental Mechanistic Studies of Methyl Oleate Ethenolysis with the First-Generation Grubbs Catalyst. *Organometallics* **2004**, *23*, 2027−2047.

(7) (a) Bailey, G. A.; Foscato, M.; Higman, C. S.; Day, C. S.; Jensen, V. R.; Fogg, D. E. Bimolecular Coupling as a Vector for Decomposition of Fast-Initiating Olefin Metathesis Catalysts. *J. Am. Chem. Soc.* **2018**, *140*, 6931−6944. For kinetics evidence, see: (b) Thiel, V.; Wannowius, K.-J.; Wolff, C.; Thiele, C. M.; Plenio, H. Ring-Closing Metathesis Reactions: Interpretation of Conversion−Time Data. *Chem. − Eur. J.* **2013**, *19*, 16403−16414.

(8) (a) Romero, P. E.; Piers, W. E. Mechanistic Studies on 14-Electron Ruthenacyclobutanes: Degenerate Exchange with Free Ethylene. *J. Am. Chem. Soc.* **2007**, *129*, 1698−1704. For additional experimental and computational evidence, see: (b) Nizovtsev, A. V.; Afanasiev, V. V.; Shutko, E. V.; Bespalova, N. B. Metathesis Catalysts Stability and Decomposition Pathway. In *Metathesis Chemistry*; Imamoglu, Y. et al., Eds.; NATO Science Series; Springer, 2007; Vol. *243*, pp 125−135. (c) Janse van Rensburg, W. J.; Steynberg, P. J.; Meyer, W. H.; Kirk, M. M.; Forman, G. S. DFT Prediction and Experimental Observation of Substrate-Induced Catalyst Decomposition in Ruthenium-Catalyzed Olefin Metathesis. *J. Am. Chem. Soc.* **2004**, *126*, 14332−14333.

(9) Nascimento, D. L.; Fogg, D. E. Origin of the Breakthrough Productivity of Ruthenium-CAAC Catalysts in Olefin Metathesis (CAAC = Cyclic Alkyl Amino Carbene). *J. Am. Chem. Soc.* **2019**, *141*, 19236−19240.

(10) (a) Smit, W.; Foscato, M.; Occhipinti, G.; Jensen, V. R. Ethylene-Triggered Formation of Ruthenium Alkylidene from Decomposed Catalyst. *ACS Catal.* **2020**, *10*, 6788−6797. (b) Engel, J.; Smit, W.; Foscato, M.; Occhipinti, G.; Törnroos, K. W.; Jensen, V. R. Loss and Reformation of Ruthenium Alkylidene: Connecting Olefin Metathesis, Catalyst Deactivation, Regeneration, and Isomerization. *J. Am. Chem. Soc.* **2017**, *139*, 16609−16619. For details of the instability of the p-cymene starting complex, see: (c) Day, C. S.; Fogg, D. E. High-Yield Synthesis of a Long-Sought, Labile Ru-NHC Complex and Its Application to the Concise Synthesis of Second-Generation Olefin Metathesis Catalysts. *Organometallics* **2018**, *37*, 4551−4555. For prior efforts aimed at catalyst regeneration, see: (d) Tabari, D. S.; Tolentino, D. R.; Schrodi, Y. Reactivation of a Ruthenium-Based Olefin Metathesis Catalyst. *Organometallics* **2013**, *32*, 5−8.

(11) (a) Zhang, J.; Song, S.; Wang, X.; Jiao, J.; Shi, M. Ruthenium-Catalyzed Olefin Metathesis Accelerated by the Steric Effect of the Backbone Substituent in Cyclic (Alkyl)(Amino) Carbenes. *Chem. Commun.* **2013**, *49*, 9491−9493. (b) Marx, V. M.; Sullivan, A. H.; Melaimi, M.; Virgil, S. C.; Keitz, B. K.; Weinberger, D. S.; Bertrand,

G.; Grubbs, R. H. Cyclic Alkyl Amino Carbene (CAAC) Ruthenium Complexes as Remarkably Active Catalysts for Ethenolysis. *Angew. Chem., Int. Ed.* **2015**, *54*, 1919−1923. (c) Gawin, R.; Kozakiewicz, A.; Guńka, P. A.; Dąbrowski, P.; Skowerski, K. Bis(Cyclic Alkyl Amino Carbene) Ruthenium Complexes: A Versatile, Highly Efficient Tool for Olefin Metathesis. *Angew. Chem., Int. Ed.* **2017**, *56*, 981−986. (d) Gawin, R.; Tracz, A.; Chwalba, M.; Kozakiewicz, A.; Trzaskowski, B.; Skowerski, K. Cyclic Alkyl Amino Ruthenium Complexes—Efficient Catalysts for Macrocyclization and Acrylonitrile Cross Metathesis. *ACS Catal.* **2017**, *7*, 5443−5449. (e) Nascimento, D. L.; Gawin, A.; Gawin, R.; Guńka, P. A.; Zachara, J.; Skowerski, K.; Fogg, D. E. Integrating Activity with Accessibility in Olefin Metathesis: An Unprecedentedly Reactive Ruthenium-Indenylidene Catalyst Bearing a Cyclic Alkyl Amino Carbene. *J. Am. Chem. Soc.* **2019**, *141*, 10626−10631. (f) Kajetanowicz, A.; Chwalba, M.; Gawin, A.; Tracz, A.; Grela, K. Non-Glovebox Ethenolysis of Ethyl Oleate and FAME at Larger Scale Utilizing a Cyclic (Alkyl)(Amino)Carbene Ruthenium Catalyst. *Eur. J. Lipid Sci. Technol.* **2019**, No. 1900263. (g) Butilkov, D.; Frenklah, A.; Rozenberg, I.; Kozuch, S.; Lemcoff, N. G. Highly Selective Olefin Metathesis with CAAC-Containing Ruthenium Benzylidenes. *ACS Catal.* **2017**, *7*, 7634−7637.

(12) (a) Lysenko, Z.; Maughon, B. R.; Mokhtar-Zadeh, T.; Tulchinsky, M. L. Stability of the First-Generation Grubbs Metathesis Catalyst in a Continuous Flow Reactor. *J. Organomet. Chem.* **2006**, *691*, 5197−5203. (b) Monfette, S.; Eyholzer, M.; Roberge, D. M.; Fogg, D. E. Getting RCM Off the Bench: Reaction-Reactor Matching Transforms Metathesis Efficiency in the Assembly of Large Rings. *Chem. − Eur. J.* **2010**, *16*, 11720−11725. (c) Skowerski, K.; Czarnocki, S. J.; Knapkiewicz, P. Tube-In-Tube Reactor as a Useful Tool for Homo- and Heterogeneous Olefin Metathesis under Continuous Flow Mode. *ChemSusChem* **2014**, *7*, 536−542.

(13) We recently demonstrated that certain **C1** catalysts resist decomposition by O_2 better than their H_2IMes analogues. See (a): Ton, S. J.; Fogg, D. E. The Impact of Oxygen on Leading and Emerging Ru-Carbene Catalysts for Olefin Metathesis: An Unanticipated Correlation Between Robustness and Metathesis Activity. *ACS Catal.* **2019**, *9*, 11329−11334. The more facile attack of sodium cyanoborohydride on **HII**, vs a CAAC analogue, has also been reported. See: ref 11g. More typically, contaminants are already present. Impurities in standard grades of ethylene, for example, were proposed to account for the higher productivity of CAAC catalysts bearing **C1**, relative to **C2** derivatives, in oleate ethenolysis. See: ref 11e. In striking contrast to the superiority of CAAC vs NHC catalysts in this reaction (see: ref 11a), H_2IMes catalysts greatly outperformed CAAC catalysts in ethenolysis of maleates. Whether this is due to impurities was not examined, however. See: (b) Engl, P. S.; Tsygankov, A.; Silva, J. D. J.; Lange, J.-P.; Copéret, C.; Togni, A.; Fedorov, A. Acrylate Esters by Ethenolysis of Maleate Esters with Ru Metathesis Catalysts: an HTE and a Technoeconomic Study. *Helv. Chim. Acta* **2020**, *103*, No. e2000035.

(14) (a) Nicola, T.; Brenner, M.; Donsbach, K.; Kreye, P. First Scale-Up to Production Scale of a Ring Closing Metathesis Reaction Forming a 15-Membered Macrocycle as a Precursor of an Active Pharmaceutical Ingredient. *Org. Process Res. Dev.* **2005**, *9*, 513−515. (b) Wang, H.; Goodman, S. N.; Dai, Q.; Stockdale, G. W.; Clark, W. M. Development of a robust ring-closing metathesis reaction in the synthesis of SB-462795, a cathepsin K inhibitor. *Org. Process Res. Dev.* **2008**, *12*, 226−234. These discoveries were made in campaigns using Hoveyda-class catalysts, $RuCl_2(L)[{=}CH(C_6H_4\text{-}2\text{-}O^iPr)$. The impact of morpholine was seen for the first-generation catalyst (L = PCy_3); that of DBU with its second-generation variant (L = H_2IMes).

(15) Vitaku, E.; Smith, D. T.; Njardarson, J. T. Analysis of the Structural Diversity, Substitution Patterns, and Frequency of Nitrogen Heterocycles among U.S. FDA Approved Pharmaceuticals. *J. Med. Chem.* **2014**, *57*, 10257−10274.

(16) (a) Compain, P.; Hazelard, D. Synthesis of Amine-Containing Heterocycles by Metathesis Reactions: Recent Advances and Opportunities. *Top. Heterocycl. Chem.* **2017**, *47*, 111−154. (b) Compain, P. Olefin Metathesis of Amine-Containing Systems: Beyond the Current Consensus. *Adv. Synth. Catal.* **2007**, *349*, 1829−1846. For additional examples cited in review articles, see: (c) Deiters, A.; Martin, S. F. Synthesis of Oxygen- and Nitrogen-Containing Heterocycles by Ring-Closing Metathesis. *Chem. Rev.* **2004**, *104*, 2199−2238. For an early report noting the importance of protecting groups in RCM of amine-containing substrates, see: (d) Nguyen, S. T.; Grubbs, R. H.; Ziller, J. W. Synthesis and Activities of New Single-Component Ruthenium-Based Olefin Metathesis Catalysts. *J. Am. Chem. Soc.* **1993**, *115*, 9858−9859.

(17) (a) Lafaye, K.; Bosset, C.; Nicolas, L.; Gue′rinot, A.; Cossy, J. Lewis Basicity Modulation of N-Heterocycles: A Key for Successful Cross-Metathesis. *Beilstein J. Org. Chem.* **2015**, *11*, 2223−2241. (b) Lafaye, K.; Nicolas, L.; Guérinot, A.; Reymond, S.; Cossy, J. Lewis Basicity Modulation of N-Heterocycles: A Key for Successful Cross-Metathesis. *Org. Lett.* **2014**, *16*, 4972−4975.

(18) (a) Bailey, G. A.; Lummiss, J. A. M.; Foscato, M.; Occhipinti, G.; McDonald, R.; Jensen, V. R.; Fogg, D. E. Decomposition of Olefin Metathesis Catalysts by Brønsted Base: Metallacyclobutane Deprotonation as a Primary Deactivating Event. *J. Am. Chem. Soc.* **2017**, *139*, 16446−16449. (b) Ireland, B. J.; Dobigny, B. T.; Fogg, D. E. Decomposition of a Phosphine-Free Metathesis Catalyst by Amines and Other Nitrogen Bases: Metallacyclobutane Deprotonation as a Major Deactivation Pathway. *ACS Catal.* **2015**, *5*, 4690−4698.

(19) For competing nucleophilic abstraction of the methylidene ligand by $NH_2{}^nBu$, see: Lummiss, J. A. M.; Botti, A. G. G.; Fogg, D. E. Isotopic Probes for Ruthenium-Catalyzed Olefin Metathesis. *Catal. Sci. Technol.* **2014**, *4*, 4210−4218.

(20) (a) Lummiss, J. A. M.; McClennan, W. L.; McDonald, R.; Fogg, D. E. Donor-Induced Decomposition of the Grubbs Catalysts: An Intercepted Intermediate. *Organometallics* **2014**, *33*, 6738−6741. and spectroscopically (see: (b) McClennan, W. L.; Rufh, S. A.; Lummiss, J. A. M.; Fogg, D. E. A General Decomposition Pathway for Phosphine-Stabilized Metathesis Catalysts: Lewis Donors Accelerate Methylidene Abstraction. *J. Am. Chem. Soc.* **2016**, *138*, 14668−14677.) This pathway can culminate in abstraction of the methylidene moiety as $[MePCy_3]Cl$. See: (c) Hong, S. H.; Wenzel, A. G.; Salguero, T. T.; Day, M. W.; Grubbs, R. H. Decomposition of Ruthenium Olefin Metathesis Catalysts. *J. Am. Chem. Soc.* **2007**, *129*, 7961−7968. For evidence of this pathway in catalysis, see: (d) Lummiss, J. A. M.; Ireland, B. J.; Sommers, J. M.; Fogg, D. E. Amine-Mediated Degradation in Olefin Metathesis Reactions that Employ the Second-Generation Grubbs Catalysts. *ChemCatChem* **2014**, *6*, 459−463.

(21) Higman, C. S.; Nascimento, D.; Ireland, B. J.; Audorsch, S.; Bailey, G. A.; McDonald, R.; Fogg, D. E. Chelate-Assisted Ring-Closing Metathesis: A Strategy for Accelerating Macrocyclization at Ambient Temperatures. *J. Am. Chem. Soc.* **2018**, *140*, 1604−1607.

(22) (a) Lee, K. L.; Goh, J. B.; Martin, S. F. *Tetrahedron Lett.* **2001**, *42*, 1635−1638. Here the failed metathesis of an exocyclic alkene could be predicted solely from the unreactivity of the first-generation Grubbs catalyst **GI** with geminally-substituted olefins. For a discussion, see: (b) van Lierop, B. J.; Lummiss, J. A. M.; Fogg, D. E. Ring-Closing Metathesis. In *Olefin Metathesis—Theory and Practice*; Grela, K., Ed.; Wiley: Hoboken, NJ, 2014; pp 85−152. In other cases, catalyst deactivation may be independent of the amine. For example, the failure of a NHC-binaphtholate catalyst in RCM synthesis of *N*-methylpiperidine derivatives (see: (c) Cortez, G. A.; Schrock, R. R.; Hoveyda, A. H. Efficient Enantioselective Synthesis of Piperidines through Catalytic Asymmetric Ring-Opening/Cross-Metathesis Reactions. *Angew. Chem., Int. Ed.* **2007**, *46*, 4534−4538) could reflect MCB deprotonation by an intramolecular Bronsted base (as established in ref 18), but may alternatively be due to formation of a metathesis-inactive piano-stool complexes. See: (d) Snelgrove, J. L.; Conrad, J. C.; Eelman, M. D.; Moriarty, M. M.; Yap, G. P. A.; Fogg, D. E. Inhibiting σ-π Isomerization of Aryloxide Ligands in Late Transition-Metal Complexes. *Organometallics* **2005**, *24*, 103−109. Tertiary *N*-allylamines, however, appear genuinely susceptible to deallylation, albeit typically in refluxing toluene with high loadings of **GI** (5 mol %). **GII** is reportedly less effective. See (b) and:

https://dx.doi.org/10.1021/acscatal.0c02760
ACS Catal. 2020, 10, 11623−11633

(e) Alcaide, B.; Almendros, P.; Luna, A. Grubbs' Ruthenium-Carbenes Beyond the Metathesis Reaction: Less Conventional Non-Metathetic Utility. *Chem. Rev.* **2009**, *109*, 3817−3858.
(23) Cox, B. G. *Acids and Bases: Solvent Effects on Acid−Base Strength*; Oxford University Press: Croydon, 2013; pp 99−115.
(24) Disappearance of the methylidene signal for **Ru-2′**, $RuCl_2(C1)(py)(=CH_2)$, was complete in <5 min at 23 °C in $CDCl_3$, at which point 98% of the H_2IMes analogue **Ru-2** remained. The latter complex was still observable after 3 h (5% vs internal standard). In both cases, ca. 80% ethylene was ultimately detected, confirming that decomposition occurs via bimolecular coupling. This is a lower limit, owing to loss of ethylene to the headspace.
(25) The beneficial impact of NEt_3 disappeared when the proportion of base was increased from 1 to 10 equiv vs **nGC1**. Specifically, the TON dropped by 4000.
(26) Lübbe, C.; Dumrath, A.; Neumann, H.; Schäffer, M.; Zimmermann, R.; Beller, M.; Kadyrov, R. How Important are Impurities in Catalysis? An Example from Ring-Closing Metathesis. *ChemCatChem* **2014**, *6*, 684−688.
(27) (a) Schrodi, Y.; Ung, T.; Vargas, A.; Mkrtumyan, G.; Lee, C. W.; Champagne, T. M.; Pederson, R. L.; Hong, S. H. Ruthenium Olefin Metathesis Catalysts for the Ethenolysis of Renewable Feedstocks. *Clean Soil, Air, Water* **2008**, *36*, 669−673. The difference is less dramatic in macrocyclization of prolactones, where the maximum reported TONs reach 62 000 for a CAAC catalyst (ref 11d). In comparison, the maximum TON reported for an NHC catalyst (albeit under stringent conditions of ethylene removal and solvent/substrate purification) is 11 100. See: (b) Kadyrov, R. Low Catalyst Loading in Ring-Closing Metathesis Reactions. *Chem. − Eur. J.* **2013**, *19*, 1002−1012.
(28) Rufh, S.; Goudreault, A. Y.; Foscato, M.; Jensen, V. R.; Fogg, D. E. Rapid Decomposition of Olefin Metathesis Catalysts by a Truncated N-Heterocyclic Carbene (NHC): Unprecedentedly Efficient Catalyst Quenching and NHC Vinylation. *ACS Catal.* **2018**, *8*, 11822−11826.
(29) (a) Melaimi, M.; Jazzar, R.; Soleilhavoup, M.; Bertrand, G. Cyclic (Alkyl)(amino)carbenes (CAACs): Recent Developments. *Angew. Chem., Int. Ed.* **2017**, *56*, 10046−10068. (b) Soleilhavoup, M.; Bertrand, G. Cyclic (Alkyl)(Amino)Carbenes (CAACs): Stable Carbenes on the Rise. *Acc. Chem. Res.* **2015**, *48*, 256−266.
(30) Paul, U. S. D.; Radius, U. What Wanzlick Did Not Dare To Dream: Cyclic (Alkyl)(amino)carbenes (cAACs) as New Key Players in Transition-Metal Chemistry. *Eur. J. Inorg. Chem.* **2017**, 3362−3375.
(31) Munz, D. Pushing Electrons: Which Carbene Ligand for Which Application? *Organometallics* **2018**, *37*, 275−289.
(32) Tolman, C. A. Steric effects of phosphorus ligands in organometallic chemistry and homogeneous catalysis. *Chem. Rev.* **1977**, *77*, 313−348.
(33) (a) Paul, U. S. D.; Sieck, C.; Haehnel, M.; Hammond, K.; Marder, T. B.; Radius, U. Cyclic (Alkyl)(Amino)Carbene Complexes of Rhodium and Nickel and Their Steric and Electronic Parameters. *Chem. − Eur. J.* **2016**, *22*, 11005−11014. (b) Dorta, R.; Stevens, E. D.; Scott, N. M.; Costabile, C.; Cavallo, L.; Hoff, C. D.; Nolan, S. P. Steric and Electronic Properties of N-Heterocyclic Carbenes (NHC): A Detailed Study on Their Interaction with $Ni(CO)_4$. *J. Am. Chem. Soc.* **2005**, *127*, 2485−2495.
(34) Fürstner, A.; Langemann, K. Macrocycles by Ring-Closing Metathesis. *Synthesis* **1997**, 792−803.
(35) Blacquiere, J. M.; Jurca, T.; Weiss, J.; Fogg, D. E. Time as a Dimension in High-Throughput Homogeneous Catalysis. *Adv. Synth. Catal.* **2008**, *350*, 2849−2855.
(36) Frisch, M. J.; Trucks, G. W.; Schlegel, H. B.; Scuseria, G. E.; Robb, M. A.; Cheeseman, J. R.; Scalmani, G.; Barone, V.; Petersson, G. A.; Nakatsuji, H.; Li, X.; Caricato, M.; Marenich, A. V.; Bloino, J.; Janesko, B. G.; Gomperts, R.; Mennucci, B.; Hratchian, H. P.; Ortiz, J. V.; Izmaylov, A. F.; Sonnenberg, J. L.; Williams; Ding, F.; Lipparini, F.; Egidi, F.; Goings, J.; Peng, B.; Petrone, A.; Henderson, T.; Ranasinghe, D.; Zakrzewski, V. G.; Gao, J.; Rega, N.; Zheng, G.; Liang, W.; Hada, M.; Ehara, M.; Toyota, K.; Fukuda, R.; Hasegawa, J.; Ishida, M.; Nakajima, T.; Honda, Y.; Kitao, O.; Nakai, H.; Vreven, T.; Throssell, K.; Montgomery, J. A., Jr.; Peralta, J. E.; Ogliaro, F.; Bearpark, M. J.; Heyd, J. J.; Brothers, E. N.; Kudin, K. N.; Staroverov, V. N.; Keith, T. A.; Kobayashi, R.; Normand, J.; Raghavachari, K.; Rendell, A. P.; Burant, J. C.; Iyengar, S. S.; Tomasi, J.; Cossi, M.; Millam, J. M.; Klene, M.; Adamo, C.; Cammi, R.; Ochterski, J. W.; Martin, R. L.; Morokuma, K.; Farkas, O.; Foresman, J. B.; Fox, D. J. *Gaussian16*, revision B.01; Gaussian, Inc.: Wallingford, CT, 2016.
(37) Frisch, M. J.; Trucks, G. W.; Schlegel, H. B.; Scuseria, G. E.; Robb, M. A.; Cheeseman, J. R.; Scalmani, G.; Barone, V.; Petersson, G. A.; Nakatsuji, H.; Li, X.; Caricato, M.; Marenich, A. V.; Bloino, J.; Janesko, B. G.; Gomperts, R.; Mennucci, B.; Hratchian, H. P.; Ortiz, J. V.; Izmaylov, A. F.; Sonnenberg, J. L.; Williams; Ding, F.; Lipparini, F.; Egidi, F.; Goings, J.; Peng, B.; Petrone, A.; Henderson, T.; Ranasinghe, D.; Zakrzewski, V. G.; Gao, J.; Rega, N.; Zheng, G.; Liang, W.; Hada, M.; Ehara, M.; Toyota, K.; Fukuda, R.; Hasegawa, J.; Ishida, M.; Nakajima, T.; Honda, Y.; Kitao, O.; Nakai, H.; Vreven, T.; Throssell, K.; Montgomery, J. A., Jr.; Peralta, J. E.; Ogliaro, F.; Bearpark, M. J.; Heyd, J. J.; Brothers, E. N.; Kudin, K. N.; Staroverov, V. N.; Keith, T. A.; Kobayashi, R.; Normand, J.; Raghavachari, K.; Rendell, A. P.; Burant, J. C.; Iyengar, S. S.; Tomasi, J.; Cossi, M.; Millam, J. M.; Klene, M.; Adamo, C.; Cammi, R.; Ochterski, J. W.; Martin, R. L.; Morokuma, K.; Farkas, O.; Foresman, J. B.; Fox, D. J. *Gaussian 16*, revision C.01; Gaussian, Inc.: Wallingford, CT, 2016.
(38) *Spartan 16*; Wavefunction, Inc.: Irvine, CA, 2016.
(39) Halgren, T. A. Merck molecular force field. I. Basis, form, scope, parameterization, and performance of MMFF94. *J. Comput. Chem.* **1996**, *17*, 490−519.
(40) Chai, J.-D.; Head-Gordon, M. Long-range corrected hybrid density functionals with damped atom-atom dispersion corrections. *Phys. Chem. Chem. Phys.* **2008**, *10*, 6615−6620.
(41) Minenkov, Y.; Singstad, Å.; Occhipinti, G.; Jensen, V. R. The Accuracy of DFT-Optimized Geometries of Functional Transition Metal Compounds: A Validation Study of Catalysts for Olefin Metathesis and Other Reactions in The Homogeneous Phase. *Dalton Trans.* **2012**, *41*, 5526−5541.
(42) Peterson, K. A.; Figgen, D.; Dolg, M.; Stoll, H. Energy-consistent relativistic pseudopotentials and correlation consistent basis sets for the 4d elements Y−Pd. *J. Chem. Phys.* **2007**, *126*, No. 124101.
(43) Energy-Consistent Pseudopotentials of the Stuttgart/Cologne Group. http://www.tc.uni-koeln.de/PP/clickpse.en.html.
(44) Dunning, T. H. Gaussian Basis Sets for Use in Correlated Molecular Calculations. I. The Atoms Boron Through Neon and Hydrogen. *J. Chem. Phys.* **1989**, *90*, 1007−1023.
(45) Schuchardt, K. L.; Didier, B. T.; Elsethagen, T.; Sun, L.; Gurumoorthi, V.; Chase, J.; Li, J.; Windus, T. L. Basis Set Exchange: A Community Database for Computational Sciences. *J. Chem. Inf. Model.* **2007**, *47*, 1045−1052.
(46) Ribeiro, R. F.; Marenich, A. V.; Cramer, C. J.; Truhlar, D. G. Use of Solution-Phase Vibrational Frequencies in Continuum Models for the Free Energy of Solvation. *J. Phys. Chem. B* **2011**, *115*, 14556−14562.
(47) Zhao, Y.; Truhlar, D. G. Computational characterization and modeling of buckyball tweezers: density functional study of concave−convex $\pi\cdots\pi$ interactions. *Phys. Chem. Chem. Phys.* **2008**, *10*, 2813−2818.
(48) Perdew, J. P.; Burke, K.; Ernzerhof, M. Generalized Gradient Approximation Made Simple. *Phys. Rev. Lett.* **1996**, *77*, 3865−3868.
(49) (a) Zhao, Y.; Truhlar, D. G. A New Local Density Functional for Main-Group Thermochemistry, Transition Metal Bonding, Thermochemical Kinetics, and Noncovalent Interactions. *J. Chem. Phys.* **2006**, *125*, No. 194101. (b) Zhao, Y.; Truhlar, D. G. Density Functionals with Broad Applicability in Chemistry. *Acc. Chem. Res.* **2008**, *41*, 157−167. (c) Zhao, Y.; Truhlar, D. G. Applications and Validations of the Minnesota Density Functionals. *Chem. Phys. Lett.* **2011**, *502*, 1−13.
(50) Marenich, A. V.; Cramer, C. J.; Truhlar, D. G. Universal Solvation Model Based on Solute Electron Density and on a

Continuum Model of the Solvent Defined by the Bulk Dielectric Constant and Atomic Surface Tensions. *J. Phys. Chem. B* **2009**, *113*, 6378−6396.
(51) Grimme, S.; Ehrlich, S.; Goerigk, L. Effect of the damping function in dispersion corrected density functional theory. *J. Comput. Chem.* **2011**, *32*, 1456−1465.
(52) Smith, D. G. A.; Burns, L. A.; Patkowski, K.; Sherrill, C. D. Revised Damping Parameters for the D3 Dispersion Correction to Density Functional Theory. *J. Phys. Chem. Lett.* **2016**, *7*, 2197−2203.
(53) Glendening, E. D.; Badenhoop, J. K.; Reed, A. E.; Carpenter, J. E.; Bohmann, J. A.; Morales, C. M.; Karafiloglou, P.; Landis, C. R.; Weinhold, F. *NBO 7.0*; Theoretical Chemistry Institute, University of Wisconsin: Madison, WI, 2018.

https://dx.doi.org/10.1021/acscatal.0c02760
ACS Catal. 2020, 10, 11623−11633